Phase-Sensitive Amplified Transmission Links for Improved Sensitivity and Nonlinearity Tolerance

Samuel L. I. Olsson, Bill Corcoran, *Member, IEEE*, Carl Lundström, *Member, IEEE*, Tobias A. Eriksson, Magnus Karlsson, *Member, IEEE, Fellow, OSA*, and Peter A. Andrekson, *Fellow, IEEE, Fellow, OSA*

(Invited Paper)

***Abstract*—In this paper, we investigate the properties of transmission links amplified by phase-sensitive amplifiers (PSAs). Using an analytic description, we explain the principles enabling improved sensitivity compared to conventional links amplified by phase-insensitive amplifiers (PIAs) and mitigation of nonlinear transmission distortions. We demonstrate these features using numerical simulations, and in particular, we show the possibility of efficiently mitigating both self-phase modulation (SPM)-induced distortions and nonlinear phase noise (NLPN) if the link dispersion map is optimized. The properties of the noise on signal and idler are important and to enable NLPN mitigation, the noise must be correlated at the link input. We investigate the role of the dispersion map in detail and show that in a link with standard single mode fiber (SSMF) the optimum dispersion map for efficient nonlinearity mitigation corresponds to precompensation of an amount equal to the effective loss length. Furthermore, we experimentally demonstrate both improved sensitivity and mitigation of nonlinearities in a 105 km PSA-amplified link transmitting 10 GBd 16-ary quadrature amplitude modulation (16QAM) data. We measure a combined effect allowing for more than 12 dB larger span loss in a PSA-amplified link compared to a conventional PIA-amplified link to reach the same bit error ratio (BER) of 1×10^{-3}.**

***Index Terms*—Fiber nonlinearity mitigation, fiber optical parametric amplifiers (FOPAs), optical amplifiers, optical fiber communication, phase-conjugated twin waves, phase-sensitive amplifiers (PSAs).**

I. Introduction

In fiber optical transmission systems, signal degradation due to amplifier noise and fiber nonlinearities limits the achievable transmission distance and channel capacity [1]–[3]. Amplifier noise will accumulate throughout the link and degrade the optical signal-to-noise ratio (OSNR), while fiber nonlinearities distort the signal through intra-channel and inter-channel effects. Intra-channel effects include signal-signal interaction resulting in self-phase modulation (SPM) and signal-noise interaction giving rise to nonlinear phase noise (NLPN) [4]. In the case of wavelength division multiplexing (WDM) transmission inter-channel effects will result in cross-phase modulation (XPM), four-wave mixing (FWM), and additional NLPN.

The OSNR degradation due to amplifier noise can be reduced by using low-noise optical amplifiers and for this reason phase-sensitive amplifiers (PSAs) have recently attracted much interest [5]. The quantum limited noise figure (NF) of PSAs is 0 dB [6], which should be compared to conventional phase-insensitive amplifiers (PIAs) such as erbium-doped fiber amplifiers (EDFAs), semiconductor optical amplifier, and Raman amplifiers (RAs) with a 3 dB quantum limited NF [7]. Implemented as inline amplifiers in a transmission link using the so-called copier-PSA scheme, PSAs are predicted to provide up to 6 dB link NF improvement compared to using conventional PIAs [8].

Several methods have been proposed for mitigating nonlinear transmission distortions such as mid-span optical phase conjugation (OPC) [9], and digital backward propagation (DBP) [10]. More recently it was shown that nonlinear distortions can also be mitigated by co-propagating two phase-conjugated waves and then coherently superimposing them at the receiver side, either in digital signal processing (DSP) [11], [12], or all-optically using a PSA [13], [14]. PSAs thus have the potential to be used both for sensitivity improvements through low NF amplification and mitigation of nonlinear transmission distortions.

PSAs can be realized using parametric gain in either $\chi^{(2)}$ [15], or $\chi^{(3)}$ nonlinear materials [16]. In fiber optical parametric amplifiers (FOPAs) phase-sensitive (PS) parametric gain is obtained through FWM where two pump waves (frequency degenerate or nondegenerate) interact with a signal and an idler wave. For the signal and idler the interaction can be modeled in a lumped manner as a coherent addition of the signal and idler, taken at the input to the PSA and shifted to oscillate at the same frequency, with the gain provided by the pump(s).

Depending on how the frequencies of pump(s), signal, and idler waves are chosen, different amplification schemes are possible. In the case of signal and idler being frequency degenerate (the degenerate idler scheme) the signal will experience 0 dB NF amplification in one quadrature and attenuation in the orthogonal quadrature, squeezing the signal phase along the direction of the amplified quadrature [6]. This scheme has successfully

Manuscript received August 6, 2014; revised September 16, 2014; accepted October 7, 2014. Date of publication November 10, 2014; date of current version February 17, 2015. This work was supported by the European Research Council under Grant ERC-2011-AdG-291618 PSOPA and by the Wallenberg Foundation. The work of B. Corcoran was also supported in part by the ARC Centre of Excellence CUDOS under Project CE110001018.

S. L. I. Olsson, C. Lundström, T. A. Eriksson, M. Karlsson, and P. A. Andrekson are with the Department of Microtechnology and Nanoscience, Chalmers University of Technology, SE-412 96 Gothenburg, Sweden (e-mail: samuel.olsson@chalmers.se; carl.lundstrom@chalmers.se; tobias.eriksson@chalmers.se; magnus.karlsson@chalmers.se; peter.andrekson@chalmers.se).

B. Corcoran is with Department of Electrical and Computer Systems Engineering, Center for Ultrahigh-bandwidth Devices for Optical Systems, Monash University, Clayton, Vic. 3800, Australia, and also with the Department of Microtechnology and Nanoscience, Chalmers University of Technology, SE-412 96 Gothenburg, Sweden (e-mail: bill.corcoran@monash.edu).

Color versions of one or more of the figures in this paper are available online at http://ieeexplore.ieee.org.

Digital Object Identifier 10.1109/JLT.2014.2367096

been used for amplification and regeneration of binary phase-shift keying (BPSK) signals [17], [18]. However, the degenerate idler scheme is inherently single-channel, not modulation format independent, and increasingly difficult to implement with advanced modulation formats thus making it unsuitable for transmission link applications aiming for high throughput.

Another possible scheme is the nondegenerate idler scheme (signal and idler at different frequencies). This scheme is capable of multi-channel amplification and, if the idler is a conjugated copy of the signal and the noise on signal and idler is uncorrelated, 0 dB NF amplification, independent of the absolute signal phase. The nondegenerate idler scheme is thus WDM-compatible and capable of providing modulation format independent noiseless amplification. The lowest NF that has been demonstrated at high (> 10 dB) gain in a PSA implemented using a FOPA is 1.1 dB [8], significantly below the quantum limited 3 dB NF of conventional PIAs. Amplification of multi-level modulation formats, such as 16-ary quadrature amplitude modulation (16QAM), has previously been demonstrated using nondegenerate idler PSA schemes both in periodically poled lithium niobate (PPLN)-based PSAs [19], and FOPA-based PSAs [20].

For the PSA gain to be stable over time, the set of waves at the input must be frequency- and phase-locked. Furthermore, to obtain amplification of both signal quadratures in a nondegenerate idler PSA, the idler must be a conjugated copy of the signal. A practical way to obtain a PSA with the required set of waves at the input is to cascade two FOPAs [21]. The signal and high-power pump are launched into the first FOPA whereby a conjugated copy of the signal, frequency- and phase-locked to the signal and pump, will be generated at the idler wavelength through FWM. The second FOPA will then have the required set of waves at its input and operate as a PSA. This scheme is commonly referred to as the copier-PSA scheme.

It has previously been shown independently that PSA-amplified transmission links implemented using the copier-PSA scheme are capable of providing both improved sensitivity [22], and nonlinearity mitigation [13], [14]. Using 16-ary quadrature amplitude modulation (16QAM) transmission over a 105 km PSA-amplified link, we recently demonstrated experimentally that the combination of improved sensitivity and nonlinearity mitigation provide PSA-amplified links a significant performance advantage over conventional PIA-amplified links, allowing more than 10 dB larger link loss to reach the same bit error ratio (BER) of 1×10^{-3} [20].

In this paper we extend the work in [20] by explaining the principle behind the sensitivity improvement and nonlinearity mitigation analytically using a transfer matrix description. We also present extensive numerical simulations of a PSA-amplified transmission link demonstrating the sensitivity improvement and nonlinearity mitigation. Through our simulations we investigate and highlight the difference between having correlated and uncorrelated noise on signal and idler at link input. Numerical simulations are also used to study the impact of the link dispersion map on the efficiency of the nonlinearity mitigation. We also briefly discuss what can be expected in terms of sensitivity improvement and nonlinearity mitigation in the case of multi-span links and WDM systems.

The paper is organized as follows. In Section II we introduce a transfer matrix based description of parametric amplifiers and based on this description analytically explain both the principle enabling noiseless amplification, leading to improved sensitivity, and cancellation of nonlinear transmission distortions using PSAs. In Section III we present numerical simulations of a single-span, single-channel PSA-amplified transmission link. In the same section we also investigate how the efficiency of the nonlinearity mitigation depends on the link dispersion map. In Section IV we show experimental results on 16QAM transmission over a 105 km link, illustrating what can be accomplished in terms of sensitivity and nonlinearity mitigation in a practical system. In Section V we discuss our results and finally in Section VI we conclude the paper.

II. Theory and Principle

A. Transfer Matrix Description

A general two-mode parametric process with signal gain and no pump depletion can be described by the transfer matrix equation [23]

$$\begin{bmatrix} B_{\mathrm{s}} \\ B_{\mathrm{i}}^{*} \end{bmatrix} = \begin{bmatrix} \mu & \nu \\ \nu^{*} & \mu^{*} \end{bmatrix} \begin{bmatrix} A_{\mathrm{s}} \\ A_{\mathrm{i}}^{*} \end{bmatrix}, \tag{1}$$

where A represent the input wave amplitudes, B represent the output wave amplitudes, subscript s denote the signal and i denote the idler, superscript $*$ represent the complex conjugate, and μ and ν are complex transfer coefficients satisfying the relation $|\mu|^2 - |\nu|^2 = 1$. The phase of μ and ν is such that the total PSA signal gain is a function of $\cos(2\phi_p - \phi_s - \phi_i)$ where ϕ_p is the pump phase, ϕ_s the signal phase, and ϕ_i the idler phase. The exact form of μ and ν can be found in [24], but is not important for the analysis presented here. We are contented knowing that they depend on the pump power, the phase-matching, the nonlinear interaction strength, and the polarization state.

To explore the capabilities of the two-mode parametric process we will consider a few different input wave combinations.

1) $A_{\mathrm{i}} = 0$: With no idler present at the input ($A_{\mathrm{i}} = 0$) the output waves are given by

$$B_{\mathrm{s}} = \mu A_{\mathrm{s}} \quad \text{and} \quad B_{\mathrm{i}} = \nu A_{\mathrm{s}}^{*}. \tag{2}$$

In this case the parametric gain is independent of the input signal phase and the amplifier operates as a PIA. From the output wave expressions we see that signal will be amplified by

$$G_{\mathrm{PIA}} = \frac{|B_{\mathrm{s}}|^2}{|A_{\mathrm{s}}|^2} = |\mu|^2 \tag{3}$$

and that the output idler will be a conjugated copy of the input signal amplified by $|\nu|^2 = G_{\mathrm{PIA}} - 1$. This process is exemplified in Fig. 1(a) with $G_{\mathrm{PIA}} = 8$ and the phase of μ and ν equal to zero.

2) $A_{\mathrm{i}} = A_{\mathrm{s}}$: With an idler present at the input the parametric gain will depend on the input signal phase which makes the amplifier operate as a PSA. In practice this requires the interacting waves to be phase-locked in order to obtain stable gain. The case of the idler being a direct copy of the signal ($A_{\mathrm{i}} = A_{\mathrm{s}}$) is interesting since it will lead to squeezing of one signal quadrature.

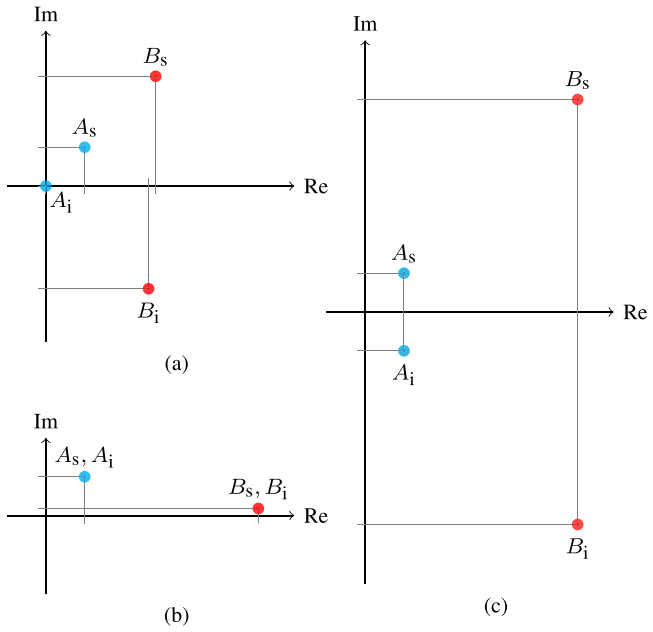

Fig. 1. Illustration of input (blue) and output (red) waves for a parametric amplifier with $|\mu|^2 = |\nu|^2 + 1 = 8$ in the case of (a) phase-insensitive operation ($A_\mathrm{i} = 0$), phase-sensitive operation with (b) $A_\mathrm{i} = A_\mathrm{s}$, and (c) $A_\mathrm{i} = A_\mathrm{s}^*$.

In this case the output waves are

$$B_\mathrm{s} = B_\mathrm{i} = (\mu + \nu)\mathrm{Re}(A_\mathrm{s}) + i(\mu - \nu)\mathrm{Im}(A_\mathrm{s}). \tag{4}$$

Given that the transfer coefficients add constructively (this can be accomplished by tuning the phase of the interacting waves [24]) the real part of the input signal will be amplified by

$$G_{\mathrm{PSA,Re}} = (|\mu| + |\nu|)^2 = 2G_\mathrm{PIA} - 1 + 2\sqrt{G_\mathrm{PIA}^2 - G_\mathrm{PIA}}, \tag{5}$$

while the imaginary part will be amplified by

$$G_{\mathrm{PSA,Im}} = 2G_\mathrm{PIA} - 1 - 2\sqrt{G_\mathrm{PIA}^2 - G_\mathrm{PIA}} = \frac{1}{G_{\mathrm{PSA,Re}}}. \tag{6}$$

This process is illustrated in Fig. 1(b). Squeezing will also be obtained in the case of $A_\mathrm{i} = -A_\mathrm{s}$, but with the output idler being the conjugate of the output signal. A degenerate idler PSA satisfies the condition $A_\mathrm{i} = A_\mathrm{s}$ and will thus give signal squeezing.

3) $A_\mathrm{i} = A_\mathrm{s}^*$: The case of the idler being a conjugated copy of the signal ($A_\mathrm{i} = A_\mathrm{s}^*$) is of particular interest since this results in amplification of both the in-phase and quadrature component of the signal. The output waves are in this case expressed as

$$B_\mathrm{s} = (\mu + \nu)A_\mathrm{s} \quad \text{and} \quad B_\mathrm{i} = (\mu + \nu)A_\mathrm{s}^*. \tag{7}$$

Both signal quadratures will be amplified by

$$G_\mathrm{PSA} = (|\mu| + |\nu|)^2 = 2G_\mathrm{PIA} - 1 + 2\sqrt{G_\mathrm{PIA}^2 - G_\mathrm{PIA}}, \tag{8}$$

which in the limit of high gain ($|\mu| \approx |\nu|$) gives us $G_\mathrm{PSA} = 4G_\mathrm{PIA}$, or in other words, the PSA gain is 6 dB higher than the PIA gain. This case is illustrated in Fig. 1(c). If $A_\mathrm{i} = -A_\mathrm{s}^*$ then both signal quadratures are attenuated.

B. Sensitivity Improvement

Up to this point we have not considered noise accompanying the signal and idler at the input of the amplifier. In the transfer matrix description noise can easily be included by adding a noise term n to the input waves

$$\begin{bmatrix} B_\mathrm{s} \\ B_\mathrm{i}^* \end{bmatrix} = \begin{bmatrix} \mu & \nu \\ \nu^* & \mu^* \end{bmatrix} \begin{bmatrix} A_\mathrm{s} + n_\mathrm{s} \\ A_\mathrm{i}^* + n_\mathrm{i}^* \end{bmatrix}, \tag{9}$$

where n_s and n_i is the noise associated with the signal and idler, respectively.

We will first discuss the case of signal and idler input waves being shot noise limited. This means that the noise accompanying the input waves is uncorrelated vacuum fluctuations. Using a semiclassical model [8], these fluctuations can be represented by additive Gaussian noise that satisfies $\langle n_m \rangle = 0$, $\langle n_m n_l \rangle = 0$, and $\langle |n_m|^2 \rangle = \hbar\omega_m/2$ with $m, l \in \{\mathrm{s}, \mathrm{i}\}$ [23]. In the general case the output waves are given by

$$B_\mathrm{s} = \mu A_\mathrm{s} + \nu A_\mathrm{i}^* + \mu n_\mathrm{s} + \nu n_\mathrm{i}^* \tag{10}$$

and

$$B_\mathrm{i} = \nu A_\mathrm{s}^* + \mu A_\mathrm{i} + \nu n_\mathrm{s}^* + \mu n_\mathrm{i}. \tag{11}$$

The uncorrelated input noise n_s and n_i will not add coherently, as can be the case for signal and idler, but instead add incoherently and thus experience a gain of

$$G_\mathrm{noise} = |\mu|^2 + |\nu|^2 = 2G_\mathrm{PIA} - 1. \tag{12}$$

Given that the signal and idler input waves are shot noise limited the output noise will be the same for all cases treated in the previous subsection, i.e. the noise at the PIA output will be the same as at the PSA output. We note that at high gain ($|\mu| \approx |\nu|$) the noise associated with the output signal and idler will be correlated and conjugated. This is of importance for the possibility to mitigate NLPN using PSAs.

Based on the signal gain and noise gain for the PIA its NF can be expressed as [24]

$$\mathrm{NF}_\mathrm{PIA} = \frac{2G_\mathrm{PIA} - 1}{G_\mathrm{PIA}}, \tag{13}$$

which in the limit of high gain ($G_\mathrm{PIA} \gg 1$) takes the value 2 (3 dB). Similarly, the NF for the quadratures amplified by the PSA (both in-phase and quadrature when $A_\mathrm{i} = A_\mathrm{s}^*$) is given by [24]

$$\mathrm{NF}_\mathrm{PSA} = \frac{2G_\mathrm{PIA} - 1}{G_\mathrm{PSA}} = \frac{2G_\mathrm{PIA} - 1}{2G_\mathrm{PIA} - 1 + 2\sqrt{G_\mathrm{PIA}^2 - G_\mathrm{PIA}}}, \tag{14}$$

which takes the value 1/2 (-3 dB) in the limit of high gain. A two-mode PSA can thus in theory provide 6 dB better sensitivity than a PIA when the input is shot noise limited. However, the improvement comes at the cost of occupying twice the bandwidth (as both signal and idler waves are required at the input) in addition to increased complexity. An alternative approach to calculating the PSA NF is to consider the total power at the PSA input, i.e. the sum of signal and idler power. In this case the NF takes the value 1 (0 dB), as predicted in [6].

TABLE I
SENSITIVITY ADVANTAGE (IN DECIBELS) FOR A TWO-CHANNEL PSA (SIGNAL AND IDLER TRANSMITTED) RELATIVE TO A SINGLE-CHANNEL PIA (SIGNAL TRANSMITTED), UNDER DIFFERENT NOISE CONDITIONS THE NOISE CAN EITHER BE FROM VACUUM FLUCTUATIONS (SHOT NOISE) OR BE INPUT (EXCESS) NOISE, AND THE LATTER CAN BE CORRELATED OR UNCORRELATED BETWEEN THE SIGNAL AND IDLER.

	Uncorrelated	Correlated
Shot noise	6 dB	-
Excess noise	3 dB	0 dB

We will now briefly discuss the case of input noise at signal and idler being dominated by incoming excess noise, as opposed to vacuum fluctuations for a shot noise limited input. The excess noise could e.g. be spontaneous emission noise from other amplifiers earlier in the system. If the excess noise on signal and idler is uncorrelated, the sensitivity advantage for the PSA over the PIA will be reduced from 6 dB to 3 dB [25]. The reason for this is that the PIA only requires the signal to be present at the input while the PSA requires both signal and idler to be present, coupling twice the amount of noise to the output modes compared to the PIA.

With correlated and conjugated excess noise at the input ($n_\mathrm{i} = n_\mathrm{s}^*$) the noise will be amplified (or attenuated) with the same gain as the signal in the PSA case while in the PIA case there will be no difference compared to having uncorrelated noise since only the noise associated with the signal wave is considered. Correlated and conjugated excess noise at the input will thus reduce the PSA sensitivity advantage by an additional 3 dB, giving the same performance as the PIA but occupying twice the bandwidth. The different cases discussed above are summarized in Table I.

In the PIA-amplified link one could consider sending the same signal at two wavelengths, so that the occupied bandwidth is the same as for the PSA-amplified link. Adding the two waves in the receiver after the PIA would result in a 3 dB sensitivity improvement compared to sending just one signal [22]. To get a sensitivity benefit from using PSAs compared to using PIAs is it thus essential that the input is shot noise limited.

When using the copier-PSA scheme to obtain improved sensitivity in a single-span link it is crucial that there is enough attenuation between the copier and the PSA to attenuate the correlated noise introduced by the copier below the level of the vacuum fluctuations. In a transmission system the link is placed between the copier and the PSA and the loss required for decorrelating the noise is thus provided by the link loss itself. This loss reduces overall link NF. However, since this loss is unavoidable in a transmission system, a copier-PSA system can be used to increase sensitivity without incurring additional penalties in a long ($> 50\,\mathrm{km}$) fiber optic link.

C. Nonlinearity Cancellation

In the simplest model, fiber nonlinearities introduce a temporal phase distortion on the signal. This approximation is broadly correct for short optical links carrying quadrature amplitude modulation (QAM) modulated signals of limited complexity

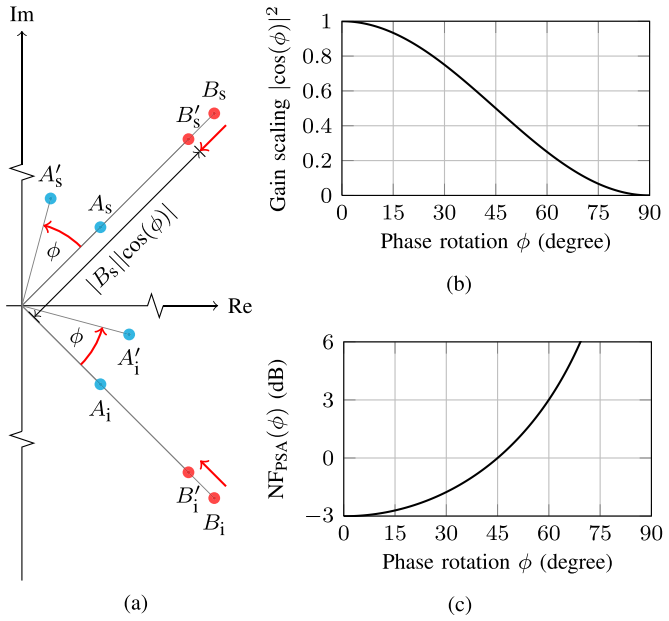

Fig. 2. PSA properties in the limit of high gain. (a) Illustration of phase rotation cancellation. (b) Signal gain reduction versus phase rotation. (c) NF versus phase rotation assuming shot noise limited input and accounting only for signal power at the PSA input.

(i.e. 16QAM and lower) [26]. In the following section we will therefore consider the case when the signal and idler, satisfying $A_\mathrm{i} = A_\mathrm{s}^*$, are rotated by an angle ϕ before being launched into the PSA. By denoting the waves after the phase rotation by primed variables we have

$$A'_\mathrm{s} = A_\mathrm{s}\exp(i\phi) \;\text{ and }\; A'_\mathrm{i} = A_\mathrm{s}^*\exp(i\phi). \tag{15}$$

At the output of the PSA we will in the limit of high gain have

$$B'_\mathrm{s} = 2\sqrt{G_\mathrm{PIA}}\cos(\phi)A_\mathrm{s} \;\text{ and }\; B'_\mathrm{i} = 2\sqrt{G_\mathrm{PIA}}\cos(\phi)A_\mathrm{s}^*. \tag{16}$$

The phase rotation ϕ will thus be canceled at the cost of reducing the gain by a factor $|\cos(\phi)|^2$. The cancellation process is illustrated in Fig. 2(a) with the gain scaling versus phase rotation plotted in Fig. 2(b). If the input is shot noise limited the gain scaling will affect the NF which can be expressed as

$$\mathrm{NF_{PSA}}(\phi) = \frac{2G_\mathrm{PIA} - 1}{G_\mathrm{PSA}|\cos(\phi)|^2}. \tag{17}$$

The PSA NF (only accounting for signal power at the PSA input) versus phase rotation is plotted in Fig. 2(c). For moderate phase rotations the impact on the NF is small. In particular we note that for phase rotations $< 15^\circ$ the NF degradation is $< 0.3\,\mathrm{dB}$.

In a single-channel PSA-amplified transmission link (with signal and idler widely spaced in frequency) intra-channel nonlinearities will dominate the nonlinear distortion. Due to signal-signal interaction the signal and idler will experience a nonlinear phase shift (from SPM) given by

$$\phi_\mathrm{NL}(t, L) = \int_0^L \gamma P(t, z)\mathrm{d}z, \tag{18}$$

where γ is the nonlinear coefficient and $P(t, z)$ the signal power. This expression can be approximated by

$$\phi_{\mathrm{NL}} = \gamma P L_{\mathrm{eff}}, \tag{19}$$

where P is the launch power and L_{eff} is the effective length defined as $L_{\mathrm{eff}} = [1 - \exp(-\alpha L)]/\alpha$ with α being the fiber attenuation and L the link length. If the phase shift is identical on both signal and idler waves it can be canceled according to the above principle when the waves are launched into the PSA. Although we expect the phase shift to be canceled independent of the degree of rotation there will be some signal degradation and distortion due to dependence of NF and gain on the phase shift. For modulation formats with multiple amplitude levels and large nonlinear phase shifts this might be visible through different levels having different gain and noise performance since $\phi_{\mathrm{NL}} \propto P$.

The signal and idler will also be distorted through signal-noise interaction which will introduce NLPN. If the amplitude noise on signal and idler is uncorrelated at the input of the link, the NLPN at the two waves after transmission will also be uncorrelated and thus add incoherently in the PSA. If, on the other hand, the amplitude noise on the two waves is correlated at the input, as can be achieved by generating the waves using a PIA, then also the NLPN will be correlated and cancellation can take place in the PSA analogous to the cancellation of an SPM induced phase shift.

D. Impact of Fiber Dispersion

The mitigation of nonlinearities through coherent summation of the signal and idler waves works best when the induced phase distortions on signal and idler waves are correlated. As such, the source of nonlinear phase distortion is important in the operation of this system. In a single-span, single-channel link, the main source of nonlinear distortions are from signal-signal interaction. This source depends on how the signal evolves as it propagates through the link. The two main effects are attenuation, which limits the length of fiber over which significant nonlinear distortion occurs, and chromatic dispersion. Chromatic dispersion drives inter symbol interference (ISI) on both the signal and idler waves, causing significant changes to the instantaneous power of these waves, resulting in a nonlinearity induced temporal distortion of the waves. However, as the signal and idler waves are phase conjugates, any phase modulated signal carried on these waves will evolve differently, causing uncorrelated nonlinear distortion on signal and idler. The dispersion map of the link thus becomes an important parameter in this system. This effect was noted in [12], where the signal and conjugate copy were transmitted on orthogonal polarizations in a multi-span link and the coherent superposition calculated in DSP after coherent detection. Assuming a symmetric link gain profile they theoretically found that the optimal dispersion map, leading to cancellation of first-order nonlinear distortions, was a 50% pre-compensation and 50% post-compensation scheme [12]. The transmission link considered in [12] differs from our copier-PSA scheme in two important ways. First, [12] has signal and conjugate waves on two polarizations at the same wavelength, which produces a different non-linear propagation environment to the copier-PSA scheme, where the signal and idler are well separated in wavelength. Second, in [12], the coherent superposition of waves happens only once at the end of the link, whereas in a copier-PSA this operation happens on a span-by-span basis. Due to these differences, we find that the balanced dispersion map is not optimal for a copier-PSA system [14], and so a new optimum configuration is sought.

III. Numerical Simulations

Numerical simulations were carried out to demonstrate the feasibility of improving sensitivity and mitigating intra-channel nonlinearities by coherent superposition. In particular we study the difference between having correlated and uncorrelated noise on the signal and idler. To understand in what systems effective nonlinearity mitigation can be obtained we investigate the impact of the dispersion map and modulation format.

A. System Model

The system model used for demonstrating mitigation of intra-channel nonlinearities and sensitivity improvements is shown in Fig. 3. A single-polarization 10 GBd 16QAM non-return-to-zero (NRZ) signal with 20 samples per symbol was generated using an IQ modulator with 28 GHz bandwidth (emulated by a Gaussian filter). The signal contained 2^{23} symbols of random data with conventional Gray coded bit-to-symbol mapping. Noise was added either before splitting and conjugation (the case of correlated noise on signal and idler) or after splitting and conjugation (the case of uncorrelated noise on signal and idler). The OSNR was set to 13 dB by adding additive white Gaussian noise (AWGN) in order to get significant signal-noise interaction in the link. The process of splitting and conjugating mimics the copier in a copier-PSA scheme.

The transmission link consisted of 100 km standard single mode fiber (SSMF) with idealized dispersion compensating fiber (DCF) for dispersion compensation. The requirement for the pre-compensation stage to induce negligible nonlinear distortion could be met by utilizing chirped fiber Bragg gratings for the pre-compensation stage [27]. The link was fully dispersion compensated but the ratio of pre- and post-compensation could be varied. Propagation in the SSMF was modeled by solving a single-polarization nonlinear Schrödinger equation using the split-step Fourier method (SSFM). We include group velocity dispersion, attenuation, and nonlinear phase terms, neglecting Raman scattering and higher order dispersion. Dispersion compensation was done in a single step neglecting attenuation and nonlinearity. We modeled the signal and idler propagation as independent based on the assumption that the signal-idler interaction is negligible in a single-channel system with signal and idler separated by about 8 nm. Initial simulations showed that the dominant effect leading to uncorrelated distortion on signal and idler is the fact that one wave is conjugated, as opposed to signal and idler propagating with different β_2. In the results presented below we used the same β_2 for signal and idler propagation for simplicity, thus ignoring higher-order dispersion. The SSMF had $\alpha = 0.25$ dB/km, $\beta_2 = 17.4\,\mathrm{ps}/(\mathrm{nm}\cdot\mathrm{km})$, and

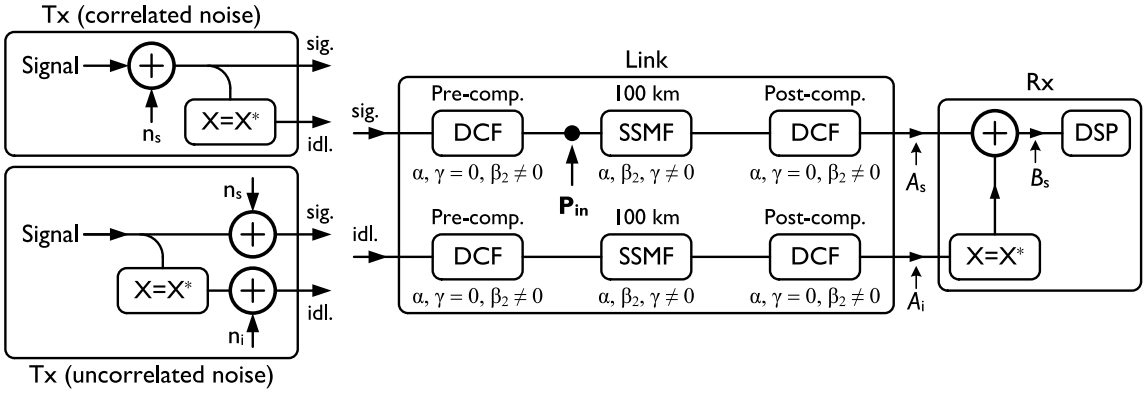

Fig. 3. System model of a dispersion compensated single-span link used for numerical simulations. DCF: dispersion compensating fiber, SSMF: standard single mode fiber, DSP: digital signal processing.

$\gamma = 1.5 \times 10^{-3} (\mathrm{W \cdot km})^{-1}$. The link launch power was taken at point $\mathrm{P_{in}}$ indicated in Fig. 3.

At the receiver end the idler was conjugated and added to the signal. This function is analogous to what a PSA does in the high-gain regime. The idler phase was rotated before begin added to the signal to maximize the optical power after addition, emulating the operation of the phase-locked loop (PLL) in an experimental system [28]. This phase adjustment was constant over all simulated symbols, mimicking the slow (kHz) response of the PLL. Finally, we use typical DSP for 16QAM with an equalizer based on decision directed least-mean square (DD-LMS) where the blind search phase estimation was performed within the DD-LMS loop [29].

B. Nonlinearity Mitigation and Sensitivity Improvement

In order to obtain optimal nonlinearity mitigation the dispersion map has to be optimized. By performing a parameter sweep of the pre- to post-compensation ratio at high launch power (10 dBm) we found that the optimal dispersion map for our system, transmitting a 10 GBd 16QAM signal over a 100 km long link with $\alpha = 0.25$ dB/km, is 20% pre-compensation and 80% post-compensation. This dispersion map corresponds to an optimum both in terms of absolute performance for the signal and idler and in terms of the improvement that is obtained by taking the superposition of the signal and the conjugate of the idler.

Simulated constellation diagrams for A_s and B_s (as defined in Fig. 3) with correlated and uncorrelated noise are shown in Fig. 4. The results for A_s were obtained by sending A_s straight to the DSP. At low launch power (0 dBm) nonlinear distortions are negligible and the difference between having correlated and uncorrelated noise on the signal and idler at the link input is only seen by a difference in OSNR after superposition. The OSNR for B_s is 3 dB higher in the case of having uncorrelated noise compared to the case of having correlated noise. At high launch power (10 dBm) nonlinear distortions are clearly visible on A_s in the form of SPM and NLPN. The clockwise rotation of the constellation is caused by the equalizer in the DSP. For B_s we clearly see that the SPM induced phase rotation is mitigated both for the case of correlated and uncorrelated noise while the NLPN is only mitigated when having correlated noise. We note

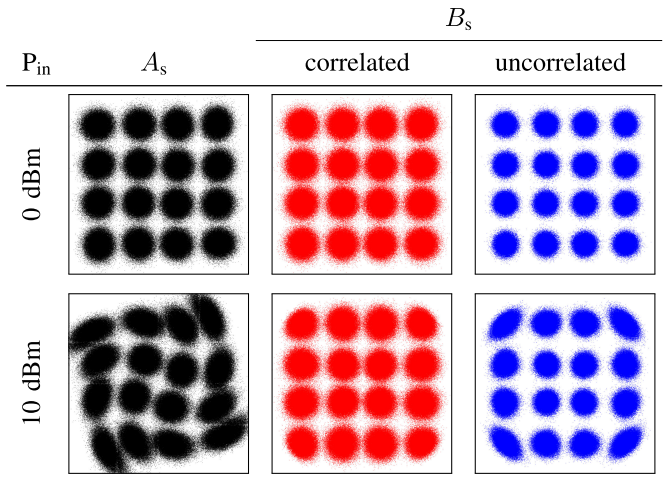

Fig. 4. Simulated constellation diagrams at 0 dBm and 10 dBm launch power with the same A_s OSNR of 13 dB illustrating the difference between A_s and B_s with correlated and uncorrelated noise on signal and idler.

that the inner-level points are slightly offset toward the center of the constellation. This effect is caused by the rotation of the idler that was done to emulate the PLL. The phase rotation maximizing the optical power tends to align the outer- and mid-level points at the cost of skewing the inner-level points. Due to the phase rotation dependence of the PSA gain [see Fig. 2(b)] the inner-level points will experience lower gain than the other points, visible in the constellation as being offset toward the center.

To quantify the benefit from the nonlinearity mitigation and OSNR improvement we calculated the BER for the transmitted data. The BER versus launch power is shown in Fig. 5. The differences seen in the constellation diagrams are reflected in the BER curves. As the launch power is increased A_s is degraded by SPM and NLPN causing a BER degradation. In the linear regime B_s with uncorrelated noise shows better performance than both A_s and B_s with correlated noise due to better OSNR. However, B_s with uncorrelated noise is successively degraded due to NLPN as the launch power is increased. B_s with

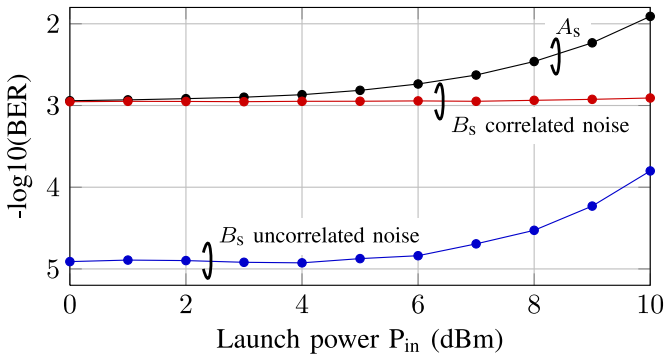

Fig. 5. Simulated BER versus launch power at 13 dB OSNR with 20% pre-compensation and 80% post-compensation corresponding to the optimal dispersion map for 10 GBd 16QAM transmission over a 100 km link.

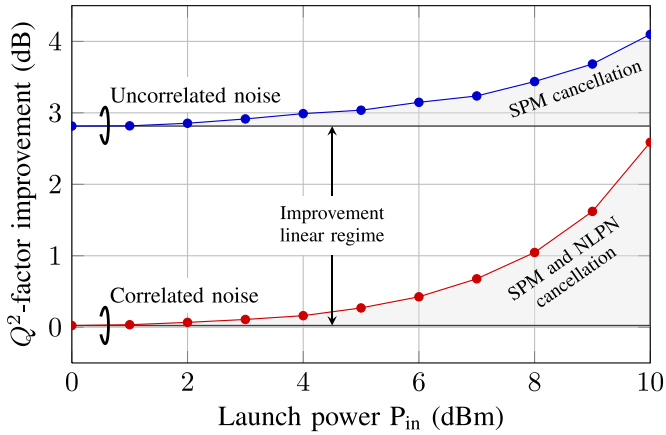

Fig. 6. Comparison of Q^2-factor improvement (difference in Q^2-factor after and before superposition) versus launch power for the case of uncorrelated and correlated noise on signal and idler.

correlated noise does not show any significant degradation as launch power is increased.

In Fig. 6 we compare the Q^2-factor improvement for B_s with uncorrelated and correlated noise versus launch power. The Q^2-factor was calculated from BER using: $Q^2 = 20\log_{10}[\sqrt{2}\mathrm{erfc}^{-1}(2\mathrm{BER})]$. For the case of correlated noise there is no improvement in the linear regime which is expected since the noise experiences the same gain as the signal. However, in the nonlinear regime significant improvement is obtained due to cancellation of both SPM and NLPN. Having uncorrelated noise on signal and idler give a clear improvement in the linear regime due to 3 dB higher signal gain than noise gain. In the nonlinear regime the improvement is smaller than for the case of correlated noise since only SPM is mitigated.

The numerical demonstration has shown the possibility of mitigating both SPM induced phase rotation and, given that the signal and idler noise is correlated at the input of the link where the nonlinearities are strong, also NLPN. Furthermore, if the noise is uncorrelated when superimposing the waves at the end of the link a benefit can also be obtained from improved OSNR.

The condition of having correlated noise in the beginning of the link and uncorrelated noise at the end of the link is in principle possible to achieve in a real system using the copier-PSA scheme. The copier will generate correlated noise on signal and idler which will generate correlated NLPN on the two waves. The attenuation from the link then decorrelates the noise on signal and idler, which can also be viewed as coupling in vacuum noise that is uncorrelated on the signal and idler [8], [16]. This enables an OSNR improvement with respect to operating with a PIA. In a link based on the copier-PSA scheme we therefore expect to see a sensitivity improvement through summing uncorrelated noise while still cancelling correlated SPM and NLPN.

In a single-span link we do not expect significant NLPN due to high OSNR at the beginning of the link. However, in a multi-span link the NLPN can become substantial as the OSNR will degrade for each span. The performance improvement from NLPN cancellation is thus expected to be more important in multi-span PSA-amplified links than in single-span PSA-amplified links. Multi-span PSA-amplified links will be discussed briefly in Section V.

C. Dispersion Map Dependence

In order to investigate how the dispersion map impacts the nonlinearity mitigation, and to ascertain the optimal dispersion map as used in the previous section, we performed numerical simulations. We used the same system model (illustrated in Fig. 3) and SSFM solver as was used to generate the results presented in the previous section. To highlight the effect of nonlinear distortions from ISI the OSNR was kept high (20 dB) and the effect of superposition was analyzed by comparing the error vector magnitudes (EVMs) of the signal with and without summation with the idler. Although EVM is perhaps not well related to BER in the case of significant phase distortion, it does give a good indication as to the behavior of the copier-PSA system.

We used a 10 GBd quadrature phase-shift keying (QPSK) signal consisting of 1310 symbols with 200 samples per symbol. The SSMF attenuation and length was varied while $\beta_2 = 17\,\mathrm{ps}/(\mathrm{nm}\cdot\mathrm{km})$ and $\gamma = 1\times10^{-3}(\mathrm{W}\cdot\mathrm{km})^{-1}$ in all cases. The noise on signal and idler was correlated.

Fig. 7 shows the EVM improvement gained by coherent summation versus pre-compensation in 80, 100, and 120 km dispersion compensated links with $\alpha = 0.22$ dB/km. The launch power was set to 15 dBm, resulting in nonlinear transmission. As the effective lengths of these links are quite similar, the magnitude of nonlinear phase shift in each case should be similar. A clear optimum pre-compensation is observed in all cases, changing slightly with length. The inset shows the result of a finer sweep around the predicted optima. This shows an optimal pre-compensation close to 25% for the 80 km link, 20% for 100 km, and 17% for 120 km.

Fig. 8 shows EVM for signal with and without superposition versus launch power in a 100 km long link that was pre-compensated, symmetrically compensated or optimally compensated. It is clear that the optimal dispersion map with 20% pre-compensation provides for the best system performance in terms of mitigation of nonlinear distortions. The change in EVM

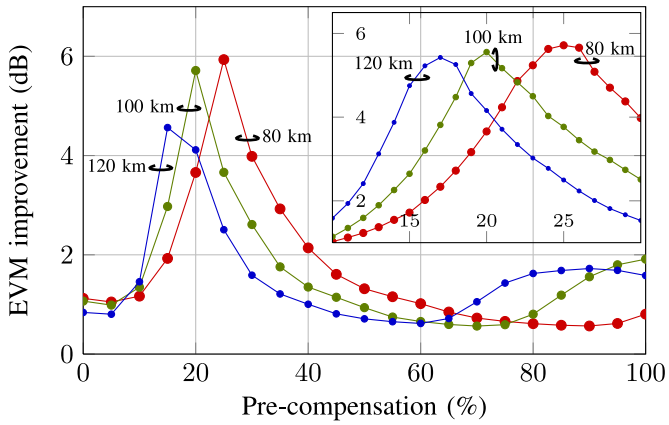

Fig. 7. EVM improvement versus pre-compensation comparing simulated output signal with and without superposition for 80, 100 and 120 km dispersion compensated links with $\alpha = 0.22$ dB/km. The launch power into the SSMF was set to 15 dBm.

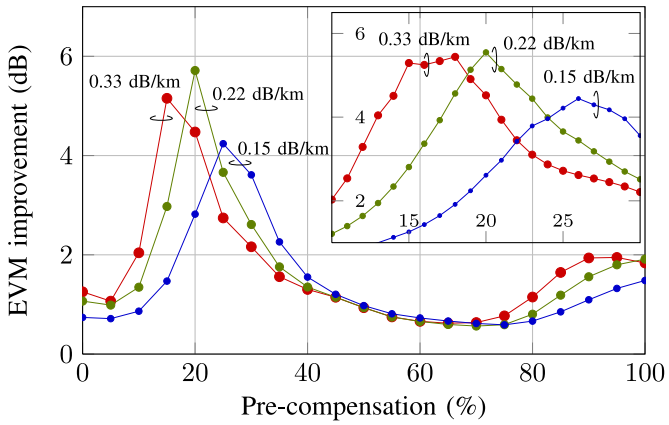

Fig. 9. EVM improvement versus pre-compensation comparing simulated output signal with and without superposition for a 100 km link with 0.15, 0.22, and 0.33 dB/km fiber attenuations. Launch power in the nonlinear regime, scaled inversely to the effective length.

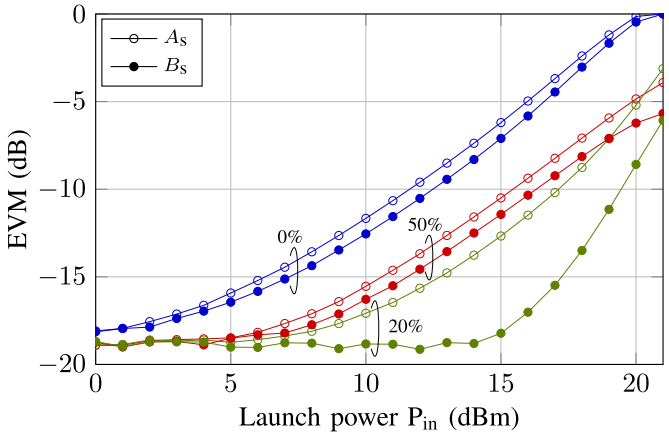

Fig. 8. Signal EVM with (B_s) and without (A_s) superposition versus launch power with various amount of pre-compensation in a 100 km dispersion compensated link with $\alpha = 0.22$ dB/km. The cases considered are 0% (post-compensation), 20% (optimal compensation), and 50% pre-compensation (symmetric map, as per [12]).

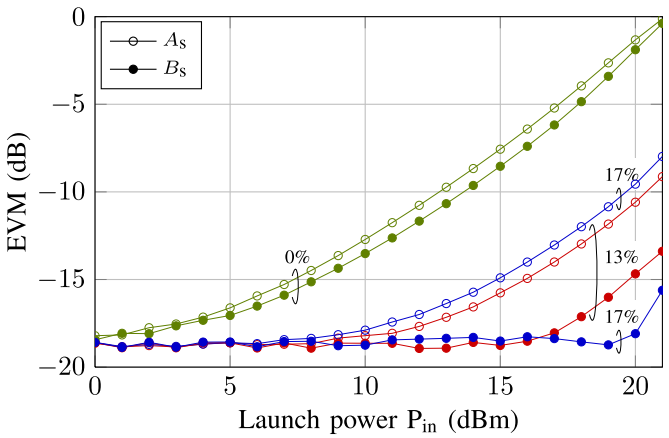

Fig. 10. Signal EVM with (B_s) and without (A_s) superposition versus launch power with various amount of pre-compensation in a 100 km dispersion compensated link with $\alpha = 0.33$ dB/km. The cases considered are 0% (post-compensation), 17% (optimal compensation), and 13% pre-compensation (corresponding to the effective length).

with varied pre-compensation in the nonlinear regime is an effect already investigated in several contexts (see e.g. [26], [30], [31]).

By calculating the DCF lengths corresponding to the optimum values of pre-compensation found in Fig. 7 we find that the optimum DCF length is constant with total link length, at a value near 20 km (340 ps/nm). This then shows that for a fiber with $\alpha = 0.22$ dB/km, the optimal lumped pre-dispersion that should be applied at the start of the span can be well characterized. We note that this optimal pre-dispersion "length" is close to the value of the maximum effective length of the fiber [32], $1/\alpha = 19.6$ km.

To investigate this further, we change the value used for attenuation in the link. Dispersion map and launch power were varied for fibres with the same properties as before, but with attenuations of 0.33, 0.22, or 0.15 dB/km. The launch power was set to 13, 15, and 17 dBm to keep the product $\gamma P L_{\text{eff}}$ similar for all attenuations. Over the 100 km span investigated, these attenuations provide effective lengths of 13.1, 19.6, and 28.0 km respectively. Fig. 9 shows the EVM improvement, with and without superposition, versus pre-compensation for the three different attenuations.

For the 0.15 and 0.22 dB/km cases, Fig. 9 shows that the optimal pre-dispersion scales reasonably well with the change in effective length, with optimal pre-dispersion "lengths" of 26 and 20 km respectively. The inset shows the result of a finer sweep around the predicted optima. For the 0.33 dB/km case, there is no clear optimum, but a range between 15–18 km. This does not scale quite so well as the other attenuation cases. We see that in the 0.33 dB/km case 13 km pre-compensation provide less improvement compared to 17 km pre-compensation. However, the EVM for the signal without superposition is better with 13 km pre-compensation than with 17 km pre-compensation as can be seen in Fig. 10 where we plot EVM for the signal with and without superposition versus launch power in a 100 km long link with 0.33 dB/km attenuation that was pre-compensated,

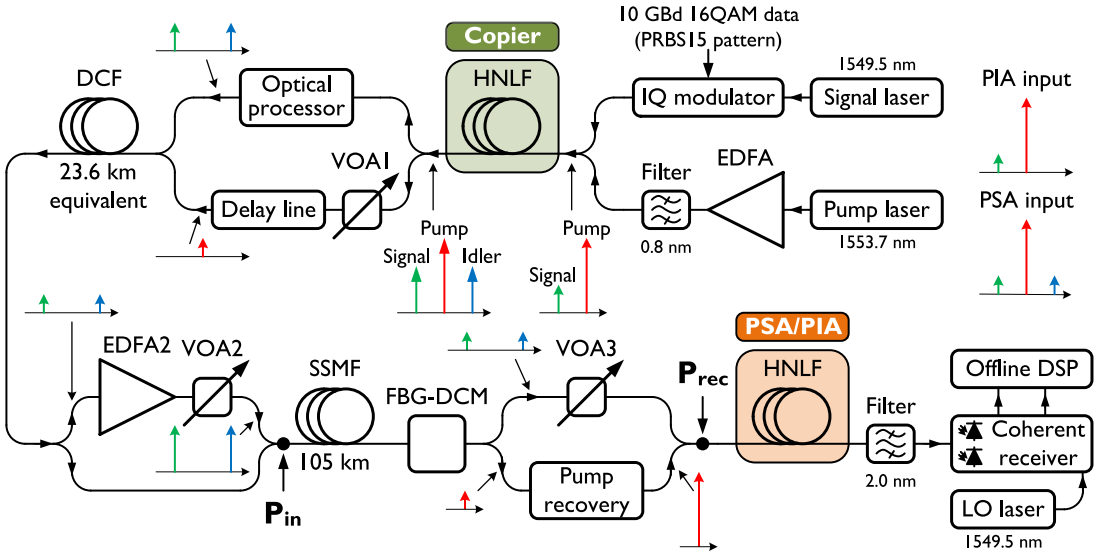

Fig. 11. Experimental setup used for demonstrating simultaneous sensitivity improvement and nonlinearity mitigation in a 10 GBd 16QAM link. EDFA: erbium-doped fiber amplifier, HNLF: highly nonlinear fiber, VOA: variable optical attenuator, DCF: dispersion compensating fiber, SSMF: standard single mode fiber, FBG-DCM: fiber Bragg-grating dispersion-compensating module, PSA: phase-sensitive amplifier, PIA: phase-insensitive amplifier, LO: local oscillator, DSP: digital signal processing.

optimally compensated, or pre-compensated with an amount corresponding to the effective length. As such it is not clear exactly how a link with higher propagation loss should be designed, preventing us from proposing a hard rule-of-thumb for design. Care should thus be taken in designing systems with higher propagation losses than SSMF.

In these simulations, the modulation format used is QPSK, as per [13], [14]. Preliminary simulations with 16QAM show a wider range of pre-compensation lengths for which the EVM improvement is close to the optimum value than what is observed with QPSK. This may be due to the increased number of different phase and amplitude states providing a greater number of possible amplitude fluctuations due to ISI, which in turn may cause some different patterns to provide similar nonlinear distortions. So, even though signal and idler are dispersed differently, the resulting ISI driven nonlinear distortion may be similar.

IV. Experimental Demonstration

To experimentally demonstrate PSAs capability of simultaneously mitigating nonlinear distortions and improving receiver sensitivity, as well as amplifying a 16QAM signal, we carried out a single-channel, single-span transmission experiment [20].

A. Experimental Setup

The experimental setup is shown in Fig. 11 and was based on previous demonstrations [14], [28]. A continuous wave (CW) laser (200 kHz linewidth) at 1549.5 nm was modulated with 10 GBd 16QAM data using an IQ-modulator and then combined with a 28 dBm CW pump at 1553.7 nm using a WDM coupler. The waves were launched into the copier which consisted of two cascaded spools of highly nonlinear fiber (HNLF) and provided a net conversion efficiency of about −5 dB, generating an idler wave at 1557.5 nm. The pump wave was then attenuated for 4 dBm launch power into the SSMF using a variable optical attenuator (VOA), VOA1, and passed through an optical delay line for equalization of the optical path undertaken by the pump wave and the signal and idler waves between the copier and the PSA. The signal and idler waves were passed through an optical processor for delay and amplitude tuning. The waves were tuned so that they had the same timing and amplitude at the PSA input. The optical processor was also used for switching between phase-insensitive (PI) and PS operation by either blocking or letting through the idler wave.

After re-combining the three waves they were launched into a DCF for pre-compensation equivalent to 23.6 km of SSMF. The powers launched into the DCF were below 0 dBm for both the signal and the idler while the pump power was about 5 dBm. The signal and idler waves were then amplified by EDFA2 and attenuated by VOA2 to set the launch power into the link. The signal launch power was measured at point P_{in} indicated in Fig. 11. The link consisted of 105 km SSMF followed by a fiber Bragg-grating dispersion-compensating module (FBG-DCM) compensating for the remainder of the link dispersion. The total link loss was 30 dB and the dispersion map was chosen based on an optimum for efficient nonlinearity mitigation found for 10 GBd QPSK data [14].

After the link the pump wave was recovered using a hybrid EDFA/injection-locking system [28], before being launched into the PIA/PSA together with the signal and idler waves. The pump recovery stage also included a PLL to stabilize the relative phase between the pump and the signal and idler against thermal drift and acoustic noise introduced by splitting the pump and the signal and idler in different paths [28]. The received signal power was varied using VOA3 and measured at point P_{rec}. Only the signal power was accounted for when measuring launch power at P_{in} and received power at P_{rec}. The PIA/PSA FOPA

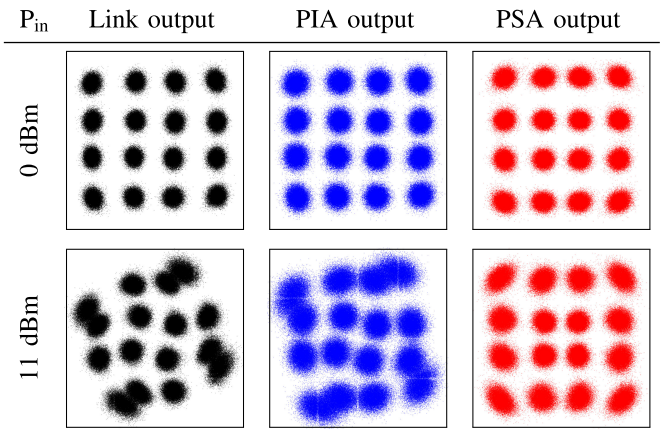

Fig. 12. Comparison of experimentally obtained 16QAM signal constellations measured at link output, PIA output, and PSA output, for the cases of 0 dBm and 11 dBm power launched into the link. The signal power into the PIA/PSA was −35 dBm.

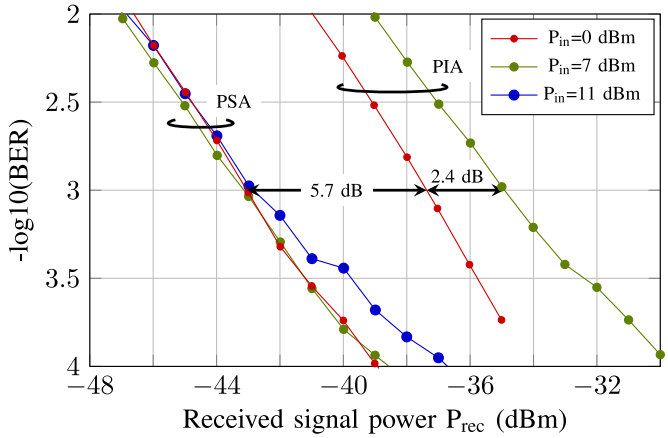

Fig. 13. Measured BER versus received power for PIA and PSA at different launch powers into the link.

was implemented with a cascade of four HNLFs similar to the one described in [33], and provided 19 dB net gain in PS-mode and 13.5 dB net gain in PI-mode.

The amplified signal was then filtered and passed to a preamplified coherent receiver where it was mixed with a 300 kHz linewidth local oscillator laser at 1549.5 nm in a 90° hybrid followed by detection and sampling using balanced photodiodes and a real-time sampling oscilloscope with 16 GHz bandwidth. We use the same DD-LMS-based DSP as was used to process the output from the numerical simulations with 16QAM. However, in this case we also included a FFT-based frequency offset estimation in the DD-LMS loop [29].

B. Experimental Results

Measured 16QAM constellations are shown in Fig. 12. Considering first the constellations measured at the link output, we see that the signal is undistorted at 0 dBm launch power while at 11 dBm launch power it shows severe nonlinear distortion. The nonlinear distortion is evident from the SPM induced rotation of the constellation, which is clearly larger for the constellation points on the outermost ring. These constellation points also suffer from more NLPN. In this case, the signal is distorted to the point that the measured BER is close to 0.5.

The constellations at PIA and PSA output were measured with −35 dBm signal power into the PIA/PSA. At 0 dBm launch power, there is a reduction in noise for the PSA case compared to the PIA case, as is expected from the lower PSA NF. The difference between the PIA and PSA cases is even clearer when the PIA/PSA input is highly distorted (at 11 dBm launch power). The result is due to the PSA being able to correct for the SPM related phase rotation. No evident NLPN reduction can be seen in the PSA case which is due to the noise at the input of the link being dominated by amplified spontaneous emission (ASE) noise added by EDFA2 which is uncorrelated at signal and idler wavelength. A slight offset of the inner-level points toward the center can be seen in the PSA case. This is caused by the PLL, as explained in connection to Fig. 4.

In Fig. 13 we compare the PIA and PSA in terms of BER versus received power P_{rec} for different signal launch powers P_{in}. At 0 dBm launch power the PSA provides 5.7 dB better sensitivity than the PIA at a BER of 1×10^{-3}. This is close to the 6 dB that we expect when signal and idler are shot noise limited at the PSA input. Increasing the signal launch power to 7 dBm no penalty can be seen for the PSA while the PIA sensitivity is degraded by about 2.4 dB at a BER of 1×10^{-3}. Further increasing the launch power to 11 dBm a small penalty can be seen for the PSA at BERs below 1×10^{-3} while for the PIA the BER was close to 0.5 for all received powers due to the strong nonlinear distortion. The PSA-amplified link thus allow for more than 12 dB larger link loss to reach the same BER of 1×10^{-3}.

V. Discussion

In this paper we have considered the case of single-span, single-channel transmission. In a WDM system we expect signal distortion not only from intra-channel nonlinear effects but also from inter-channel effects. The mitigation of nonlinear distortions in multi-channel PSA-amplified links has not yet been investigated. However, with the complete signal-band copied and conjugated to the idler wavelength we expect the signals and idlers to experience correlated distortions also from inter-channel nonlinearities thus enabling mitigation through superposition in a PSA. In [12] mitigation of inter-channel nonlinearities was demonstrated in a related twin-wave system where the superposition of signals and conjugates was carried out after coherent detection in DSP. We do however expect that in attempting to compensate for phase distortions over a wide WDM bandwidth, that the system will be more sensitive to the precise dispersion map used for the link, which is likely to limit achievable performance improvements.

Multi-span links with in-line PSAs have thus far only been demonstrated using a degenerate idler scheme [18]. This scheme is neither WDM compatible nor modulation format independent. In a multi-span link based on the copier-PSA scheme low noise amplification and nonlinearity mitigation would take place at

each PSA node, according to the principles described in this paper. Accumulation of noise would thus be reduced, as would the accumulation of signal distortions due to nonlinearity. After each amplification stage the noise on signal and idler would be correlated thus also enabling mitigation of NLPN. However, there might be other penalties associated with multi-span PSA-amplified links. In particular noise accumulation on the pump through the pump recovery system could cause performance degradation at long transmission distances [28].

The copier-PSA scheme is unique in its ability to deal with non-deterministic sources of nonlinear phase distortions, particularly NLPN. DBP cannot deal with stochastic variations, and the optical noise on the twin-waves of [12] is uncorrelated which may also hinder mitigation of NLPN. The copier-PSA scheme, however, provides correlated noise on both signal and idler, allowing for mitigation of the otherwise unpredictable NLPN.

VI. Conclusion

We have investigated the properties of PSA-amplified transmission links analytically, numerically, and experimentally. We presented a theory based on a transfer matrix approach explaining how PSAs can provide improved sensitivity compared to PIAs and the possibility of nonlinearity mitigation. We discussed how the properties of the noise on signal and idler impact the PSA sensitivity and nonlinearity mitigation.

By numerically simulating a single-span, single-channel PSA-amplified transmission link we demonstrated both improved OSNR, leading to improved sensitivity, and mitigation of SPM induced distortions as well as NLPN. The dependence of the efficiency for nonlinearity mitigation on the dispersion map was also investigated numerically and we found that for SSMF with a loss of 0.15 and 0.22 dB/km the optimal amount of pre-compensation is roughly equal to the effective length. For fiber with higher loss the optimum is slightly offset from the effective length.

We experimentally demonstrated transmission of a 10 GBd 16QAM signal over a PSA-amplified link and compared it with a PIA-amplified link. In the linear propagation regime, the PSA-amplified link showed 5.5 dB higher sensitivity than the PIA-amplified link, owing to the improved noise performance. In the nonlinear regime, the PSA is able to correct for much of the nonlinear phase rotation of the signal. This results in a recoverable signal even for large nonlinear phase shifts, that would otherwise have led to failing DSP. The combined effect of improved sensitivity and mitigation of nonlinearities allow the PSA-amplified link more than 12 dB larger link loss than a PIA-amplified to reach the same BER of 10^{-3}.

Acknowledgment

The authors would like to thank OFS Denmark for providing HNLFs and acknowledge P. Johannisson for useful discussions regarding the simulations.

References

[1] R.-J. Essiambre, G. Kramer, P. J. Winzer, G. J. Foschini, and B. Goebel, "Capacity limits of optical fiber networks," *J. Lightw. Technol.*, vol. 28, no. 4, pp. 662–701, Feb. 2010.

[2] A. D. Ellis, J. Zhao, and D. Cotter, "Approaching the non-linear Shannon limit," *J. Lightw. Technol.*, vol. 28, no. 4, pp. 423–433, Feb. 2010.

[3] E. Agrell, "Nonlinear fiber capacity," in *Proc. Eur. Conf. Exh. Opt. Commun.*, (The Institution of Engineering and Technology, 2013), We.4.D.3.

[4] J. P. Gordon and L. F. Mollenauer, "Phase noise in photonic communications systems using linear amplifiers," *Opt. Lett.*, vol. 15, no. 23, pp. 1351–1353, Dec. 1990.

[5] Z. Tong, C. Lundström, P. A. Andrekson, C. J. McKinstrie, M. Karlsson, D. J. Blessing, E. Tipsuwannakul, B. J. Puttnam, H. Toda, and L. Grüner-Nielsen,"Towards ultrasensitive optical links enabled by low-noise phase-sensitive amplifiers," *Nat. Photon.*, vol. 5, no. 7, pp. 430–436, Jun. 2011.

[6] C. M. Caves, "Quantum limits on noise in linear amplifiers," *Phys. Rev. D*, vol. 26, no. 8, pp. 1817–1839, Oct. 1982.

[7] E. Desurvire, *Erbium-Doped Fiber Amplifiers*. New York, NY, USA: Wiley, 1994.

[8] Z. Tong, C. J. McKinstrie, C. Lundström, M. Karlsson, and P. A. Andrekson, "Noise performance of optical fiber transmission links that use non-degenerate cascaded phasesensitive amplifiers," *Opt. Exp.*, vol. 18, no. 15, pp. 15426–15439, Jul. 2010.

[9] S. L. Jansen, D. van den Borne, B. Spinnler, S. Calabrò, H. Suche, P. M. Krummrich, W. Sohler, G.-D. Khoe, and H. de Waardt, "Optical phase conjugation for ultra long-haul phase-shift-keyed transmission," *J. Lightw. Technol.*, vol. 24, no. 1, pp. 54–64, Jan. 2006.

[10] E. Ip and J. M. Kahn, "Compensation of dispersion and nonlinear impairments using digital backpropagation," *J. Lightw. Technol.*, vol. 26, no. 20, pp. 3416–3425, Oct. 2008.

[11] Y. Tian, Y.-K. Huang, S. Zhang, P. R. Prucnal, and T. Wang, "Demonstration of digital phase-sensitive boosting to extend signal reach for long-haul WDM systems using optical phase-conjugated copy," *Opt. Exp.*, vol. 21, no. 4, pp. 5099–5106, Feb. 2013.

[12] X. Liu, A. R. Chraplyvy, P. J. Winzer, R. W. Tkach, and S. Chandrasekhar, "Phase-conjugated twin waves for communication beyond the Kerr nonlinearity limit," *Nat. Photon.*, vol. 7, pp. 560–568, May 2013.

[13] S. L. I. Olsson, B. Corcoran, C. Lundström, M. Sjödin, M. Karlsson, and P. A. Andrekson, "Phase-sensitive amplified optical link operating in the nonlinear transmission regime," in *Proc. Eur. Conf. Exhib. Opt. Commun.*, (Optical Society of America, Washington, DC, 2012), Th.2.F.1.

[14] B. Corcoran, S. L. I. Olsson, C. Lundström, M. Karlsson, and P. A. Andrekson, "Mitigation of nonlinear impairments on QPSK data in phase-sensitive amplified links," in *Proc. Eur. Conf. Exhib. Opt. Commun.*, (The Institution of Engineering and Technology, 2013), We.3.A.1.

[15] D. J. Lovering, J. A. Levenson, P. Vidakovic, J. Webjörn, and P. S. J. Russell, "Noiseless optical amplification in quasi-phase-matched bulk lithium niobate," *Opt. Lett.*, vol. 21, pp. 1439–1441, 1996.

[16] Z. Tong, C. Lundström, P. A. Andrekson, M. Karlsson, and A. Bogris, "Ultralow noise, broadband phase-sensitive optical amplifiers, and their applications," *IEEE J. Sel. Topics Quantum Electron.*, vol. 18, no. 2, pp. 1016–1032, Mar./Apr. 2012.

[17] R. Slavík, F. Parmigiani, J. Kakande, C. Lundström, M. Sjödin, P. A. Andrekson, R. Weerasuriya, S. Sygletos, A. D. Ellis, L. Gröner-Nielsen, D. Jakobsen, S. Herstrøm, R. Phelan, J. O′Gorman, A. Bogris, D. Syvridis, S. Dasgupta, P. Petropoulos, and D. J. Richardson, "All-optical phase and amplitude regenerator for next-generation telecommunications systems," *Nat. Photon.*, vol. 4, pp. 690–695, Oct. 2010.

[18] T. Umeki, M. Asobe, H. Takara, Y. Miyamoto, and H. Takenouchi, "Multi-span transmission using phase and amplitude regeneration in PPLN-based PSA," *Opt. Exp.*, vol. 21, no. 15, pp. 18170–18177, Jul. 2013.

[19] T. Umeki, O. Tadanaga, M. Asobe, Y. Miyamoto, and H. Takenouchi, "First demonstration of high-order QAM signal amplification in PPLN-based phase sensitive amplifier," *Opt. Exp.*, vol. 22, no. 3, pp. 2473–2482, Feb. 2014.

[20] S. L. I. Olsson, T. A. Eriksson, C. Lundström, M. Karlsson, and P. Andrekson, "Linear and nonlinear transmission of 16-QAM over 105 km phase-sensitive amplified link," in *Proc. Opt. Fiber Commun. Conf. Expo. Nat. Fiber Opt. Eng. Conf.*, (Optical Society of America, Washington, DC, 2014), Th1H.3.

[21] R. Tang, J. Lasri, P. S. Devgan, V. Grigoryan, P. Kumar, and M. Vasilyev, "Gain characteristics of a frequency nondegenerate phase-sensitive fiber-optic parametric amplifier with phase self-stabilized input," *Opt. Exp.*, vol. 13, no. 26, pp. 10483–10493, Dec. 2005.

[22] B. Corcoran, S. L. I. Olsson, C. Lundström, M. Karlsson, and P. Andrekson, "Phase-sensitive optical pre-amplifier implemented in an 80 km DQPSK link," in *Proc. Opt. Fiber Commun. Conf. Expo. Nat. Fiber Optic Eng. Conf.*, (Optical Society of America, Washington, DC, 2012), PDP5A.4.
[23] C. J. McKinstrie, S. Radic, and M. G. Raymer, "Quantum noise properties of parametric amplifiers driven by two pump waves," *Opt. Exp.*, vol. 12, no. 21, pp. 5037–5066, Oct. 2004.
[24] M. Vasilyev, "Distributed phase-sensitive amplification," *Opt. Exp.*, vol. 13, no. 19, pp. 7563–7571, Sep. 2005.
[25] B. Corcoran, R. Malik, S. L. I. Olsson, C. Lundström, M. Karlsson, and P. A. Andrekson, "Noise beating in hybrid phase-sensitive amplifier systems," *Opt. Exp.*, vol. 22, no. 5, pp. 5762–5771, Mar. 2014.
[26] R. Dar, M. Feder, A. Mecozzi, and M. Shtafi, "Accumulation of nonlinear interference noise in fiber-optic systems," *Opt. Exp.*, vol. 22, no. 12, pp. 14199–14211, Jun. 2014.
[27] E. Tipsuwannakul, J. Li, T. Eriksson, L. Egnell, F. Sjöström, J. Pejnefors, P. Andrekson, and M. Karlsson, "Influence of fiber-Bragg grating-induced group-delay ripple in high-speed transmission systems," *J. Opt. Commun. Netw.*, vol. 4, no. 6, pp. 514–521, Jun. 2012.
[28] S. L. I. Olsson, B. Corcoran, C. Lundström, E. Tipsuwannakul, S. Sygletos, A. D. Ellis, Z. Tong, M. Karlsson, and P. A. Andrekson, "Injection locking-based pump recovery for phase-sensitive amplified links," *Opt. Exp.*, vol. 21, no. 12, pp. 14512–14529, Jun. 2013.
[29] T. Pfau, S. Hoffmann, and R. Noé, "Hardware-efficient coherent digital receiver concept with feedforward carrier recovery for M-QAM constellations," *J. Lightw. Technol.*, vol. 27, no. 8, pp. 989–999, Apr. 2009.
[30] Y. Frignac, J.-C. Antona, S. Bigo, and J.-P. Hamaide, "Numerical optimization of pre- and in-line dispersion compensation in dispersion-managed systems at 40 Gbit/s," in *Proc. Opt. Fiber Commun. Conf. Expo. Nat. Fiber Opt. Eng. Conf.*, (Optical Society of America, Washington, DC, 2002), ThFF5.
[31] M. Seimetz, M. Nölle, C.-M. Weinert, R. Freund, B. Spinnler, S. Spälter, and C. Fludger, "Influence of neighbor channel modulation formats on 112 Gbit/s and 42.8 Gbit/s WDM coherent polmux-QPSK transmission systems," in *Proc. Opt. Fiber Commun. Conf. Expo. Nat. Fiber Opt. Eng. Conf.*, (Optical Society of America, Washington, DC, 2009), JThA44.
[32] G. Agrawal, *Nonlinear Fiber Optics*, 3rd ed. New York, NY, USA: Academic, 2001.
[33] C. Lundström, R. Malik, L. Grüner-Nielson, B. Corcoran, S. L. I. Olsson, M. Karlsson, and P. A. Andrekson, "Fiber optic parametric amplifier with 10-dB net gain without pump dithering," *IEEE Photon. Technol. Lett.*, vol. 25, no. 3, pp. 234–237, Feb. 2013.

Samuel L. I. Olsson was born in Katrineholm, Sweden, in 1984. He received the M.Sc. degree in engineering physics in 2009, and the Licentiate of Engineering degree in 2013, both from Chalmers University of Technology, Gothenburg, Sweden, where he is currently working toward the Ph.D. degree with the Photonics Laboratory.

His research interests include fiber optical parametric amplification and in particular phase-sensitive parametric amplification for transmission system applications. Other research interests include optical injection-locking.

Mr. Olsson received the best student paper award at the European Conference of Optical Communication 2012 and the honorable mention award in the Corning Outstanding Student Paper Competition at the Optical Fiber Communication Conference and Exposition 2014.

Bill Corcoran received the B.Sc. degree in physics and the B.Eng. (Hons.) degree in electronic engineering at RMIT University, Melbourne, Australia, in 2006. He received the Ph.D. degree from the University of Sydney, Sydney, Australia, on enhanced optical nonlinearities in silicon waveguides in 2011, focused mainly on "slow light" enhanced all-optical effects and functionalities in planar photonic crystal waveguides. He then held a Postdoctoral research position with the fiber optical communications group in MC2 within the Chalmers University of Technology, Gothenburg, Sweden, until mid 2013, working with phase-sensitive amplification and all-optical nonlinear processing. Since late 2013, he has been a Research Fellow with Monash University, Melbourne, Australia, working on advanced modulation formats for fibre optic communications, developing technologies to increase data rates in long-haul fibre links.

Carl Lundström (S'10–M'12) was born in Umeå, Sweden, in 1982. He received the M.Sc. degree in engineering physics in 2007 and the Ph.D. degree in 2012, both from Chalmers University of Technology, Göteborg, Sweden. The topic of his Ph.D. thesis was phase-sensitive fiber-based optical parametric amplifiers. After receiving the Ph.D. degree, he has been a Postdoctoral researcher with the Chalmers University of Technology, working on nonlinear optical signal processing and high-speed signal generation and characterization. He has authored or coauthored more than 40 scientific journal and conference papers, several of which were invited papers. He is serving as a Reviewer for the journals of IEEE and the Optical Society of America.

Tobias A. Eriksson was born in Sandviken, Sweden, in 1986. He received the M.Sc. degree in electrical engineering with a specialization in photonics from the Chalmers University of Technology, Gothenburg, Sweden, in 2011, where he is currently working toward the Ph.D. degree.

His current research interests include multidimensional modulation formats for long-haul coherent fiber optical transmission systems as well as various aspects of multicore fiber systems.

Magnus Karlsson received the Ph.D. degree from the Chalmers University of Technology, Gothenburg, Sweden, in 1994. Since 1995, he has been with the Photonics Laboratory, Chalmers University of Technology, first as an Assistant Professor and since 2003 as a Professor in photonics. He has authored or coauthored around 300 scientific journal and conference contributions in the areas of nonlinear optics and fiber optic transmission. He cofounded the Chalmers Fiber-Optic Communication Research Center FORCE in 2010. His current research interests include linear and nonlinear fiber transmission effects, and multilevel modulation in optical communication systems.

Dr. Karlsson has served in the technical committee for the Optical Fiber Communication Conference, and currently serves in the technical program committees for the European Conference of Optical Communication, and the Asia Communications and Photonics Conference. He is an Associate Editor for Optics Express since 2010. He contributed in the CELTIC 100-GET and EO-Net projects that were both awarded the gold excellence award. He supervised students receiving the best paper awards at GlobeCom 2011, and at ECOC 2012. He is appointed as a Fellow of the Optical Society of America in 2012.

Peter A. Andrekson received the Ph.D. degree from the Chalmers University of Technology, Gothenburg, Sweden, in 1988. After about three years with AT&T Bell Laboratories, Murray Hill, NJ, USA, during 1989–1992, he returned to Chalmers, where he is currently a Full Professor with the Department of Microtechnology and Nanoscience. He was a Director of Research, Cenix Inc., Allentown, PA, USA, during 2000–2003 and with the newly established Center for Optical Technologies, Lehigh University, Bethlehem, PA, USA during 2003–2004. His research interests include nearly all aspects of fiber communications such as optical amplifiers, nonlinear pulse propagation, all-optical functionalities, and very high capacity transmission. He is a cofounder of the optical test and measurement company Picosolve Inc., now part of EXFO, Quebec City, QC, Canada.

Dr. Andrekson is a Fellow of the Optical Society of America. He is the author of about 450 scientific publications and conference papers in the area of optical communications, among which more than 90 were invited papers at leading international conferences and journals, including three tutorials at the Optical Fiber Communication Conference in 2004, 2011, and 2014. He was an elected member of the Board of Governors for the IEEE Photonics Society (2011–2013) and is or has served on several technical program committees, including OFC and ECOC, and as international project and candidate evaluator, and has also twice served as an expert for the evaluation of the Nobel Prize in Physics. He was an Associate Editor for IEEE Photonics Technology Letters during 2003–2007. In 1993, he received a price from the Swedish government research committee for outstanding work performed by young scientists, and in 2000 hereceived the Telenor Nordic research award for his contribution to optical technologies.